Self-assembly and transport phenomena of colloids: confinement and geometrical effects

César O. Solano-Cabrera,[1] Pavel Castro-Villarreal,[2] Rosario E. Moctezuma,[3] Fernando Donado,[4] Jacinta C. Conrad,[5] and Ramón Castañeda-Priego [6]

[1]División de Ciencias e Ingenierías, Universidad de Guanajuato, 37150, León, Mexico
[2]Facultad de Ciencias en Física y Matemáticas, Universidad Autónoma de Chiapas, 29050, Tuxtla Gutiérrez, Mexico
[3]Instituto de Física, Universidad Autónoma de San Luis Potosí, 78290, San Luis Potosí, Mexico
[4]Instituto de Ciencias Básicas e Ingeniería, Universidad Autonóma del Estado de Hidalgo, 42184, Pachuca, Mexico
[5]William A. Brookshire Department of Chemical and Biomolecular Engineering, University of Houston, Houston, TX, 77204-4004, USA
[6]Departamento de Ingeniería Física, Universidad de Guanajuato, 37150, León, Mexico; email: ramoncp@fisica.ugto.mx

Xxxx. Xxx. Xxx. Xxx. 2025. 16:1–23

https://doi.org/10.1146/((please add article doi))

Keywords

colloids, granular matter, self-assembly, transport phenomena, confinement, non-Euclidean geometry

Abstract

Colloidal dispersions exhibit rich equilibrium and non-equilibrium thermodynamic properties, self-assemble (spontaneously or driven externally) to form a large diversity of structures at different length scales, and display interesting and complex transport behavior under bulk conditions. In confinement or under geometrical restrictions, new and interesting phenomena emerge that have no counterpart when the colloids are embedded in an open and non-curved space. In this review, we focus on the effects of confinement and geometry on the self-assembly and transport of colloids and fluidized granular systems, which serve as model systems. Our main goal is to provide a balanced discussion of the various contributions, including experiments, theoretical approximations and molecular simulations, that provide physical insight on the role played by the geometry at the mesoscopic scale. We also draw attention to some particular problems and challenges, and show preliminary results based on the covariant Smoluchowski equation, that represent promising perspectives to further study colloidal dynamics in a non-Euclidean geometry.

Contents

1. INTRODUCTION: COLLOIDS, CONFINEMENT AND GEOMETRY

Colloidal suspensions are many-body systems composed of nanometer- to micrometer-sized particles, typically named colloids, dispersed in a continuum liquid medium (the solvent). Colloids are widely used in industrial and technological applications, such as paints, foods, and medicines (1), and as feedstocks for additive manufacturing of advanced materials (2, 3). Scientifically, colloids serve as model systems to understand, for example, both the equilibrium phase behavior and non-equilibrium states of matter, effective interactions among macromolecules, the mechanical response of materials, and how the self-assembly and transport processes are affected by either confinement or geometrical restrictions (1, 4, 5). Additionally, colloids can be classified as passive or active matter depending on whether the particles are self-propelled (6).

Colloids are widely used as model systems for several reasons. First, colloids and other macromolecules share similar length scales (10 nm – 1 μm), which renders them 'visible.' As a consequence, they are relatively slow (typical time scales 1 μs - 1 s), which allows colloidal dynamics and transport processes to be followed in real time. Second, the interactions between colloidal particles, of the order of the thermal energy k_BT, also describe the interaction between macromolecules immersed in an aqueous environment and can be tuned over a broad range. Third, since colloidal interactions are relatively weak, colloids are highly susceptible to external forces that are able to spatially confine them. Thus, their properties can be controlled through the application of external modulation. Finally, colloidal suspensions can be studied at the single-particle level by means of complementary techniques, i.e., experiments, computer simulations and theoretical approximations (1, 4, 5).

"Passive colloidal matter" exhibits rich equilibrium and non-equilibrium thermodynamic behaviors when it is either spatially unconfined or geometrically constricted (5, 7). These systems can also sustain non-equilibrium dissipative structures (8). "Active colloidal dispersions," by contrast, contain particles that constantly consume energy from the environment and turn it, most of the time through complex mechanisms, into locomotion (9). Active Brownian particles, microswimmers, and layers of vibrating grains fall in this category because they all extract energy from their surroundings and transform it into mechanical work using different phoretic mechanisms (6, 10). Studying the individual behavior of self-propelled particles and the collective behavior that emerges in systems of interacting active colloidal particles, including those cases where the particles are spatially constricted, enhances understanding of the non-equilibrium nature of this kind of active matter. This knowledge thus enables fundamental first-principle frameworks for investigating the statistical physics of out-of-equilibrium systems under confinement to be built (6). More importantly, it is possible to adapt established theoretical formalisms to the case of active matter under confinement to account for the most elemental properties of dissipative matter and the non-equilibrium transport and self-assembly of materials composed of active colloidal particles that experience any type of spatial restriction, see, e.g., Refs. (6, 11, 12, 13, 14, 15, 16).

1.1. How to confine colloidal particles? Types of confinement

Confining a colloidal dispersion to a small volume or area affects its phase behavior, self-assembly, and transport properties (17, 18, 19, 20). Confinement is present in natural and artificial colloidal systems of great scientific and technological relevance (21). The degree of confinement dictates many of the phenomena observed in such colloidal systems. Other effects, however, can be attributed solely to the intrinsic confinement characteristics: topographical (hard or rigid) or energetic (soft) (22). Soft confinement refers to the lack of a well-defined width of the confining region, *i.e.*, there is not a prescribed (rigid-like) boundary that defines the available space to the particles. This kind of confinement induces different structural transitions and dynamical scenarios than those already observed with rigid confinement (21, 22, 23, 24). Confinements imposed on colloids in experiments, however, may fall between the hard and soft limits: for example, colloids confined to a liquid-liquid interface (a prescribed but deformable, fluctuating boundary), or colloids sedimented to a 2-D layer near a rigid wall (whose out-of-plane motion is suppressed by gravity but not entirely eliminated).

Most studies of confinement effects examine scenarios with rigid confining walls, *i.e.*, where the region that constrains the motion of the colloidal particles has a well-defined volume or area. For example, several studies examined crystallization of hard and soft colloids under rigid confinement, e.g., Refs. (18, 19, 20, 21, 22), and references therein. Recent works have highlighted the importance of the role played by the softness of the confining mechanism (21, 22, 23, 24, 25, 26), including, for example, the appearance of multiple relaxation regimes in glassy colloidal liquids induced by soft confinement (25).

Soft confinement can be produced by a soft repulsion between the confining walls and the particles (22, 26) or when a harmonic well confines or restricts the area or volume available to the particles (21, 25). These soft potentials can be systematically tuned to lead to either a weak or strong degree of confinement. Therefore, by playing with the softness of the potential, it is possible to suppress or enhance certain kinds of structural ordering with significant implications for the colloid dynamics (25, 27).

When one is able to manipulate the confining boundaries of the colloidal system, it is also possible to modify the energy landscape that the colloids experience. This opens up new possibilities for the self-assembly and rational design of mesoscopic clusters with a diversity of mechanical and optical properties (28). Optical traps coupled to colloidal systems are clean and excellent model systems to experimentally explore new exciting possibilities where the degree of confinement can be modified to observe new self-assembly and transport phenomena (29).

External soft potentials lead to changes in colloid structure, as shown in recent studies. For example, the effect on the structure of a hard-sphere fluid near a soft wall (26); the role played by the softness of a harmonic potential on the layering, freezing, and melting of hard colloidal particles (21); and crystallization of soft colloids in soft confinement (22). However, these contributions largely examined quasi-two-dimensional, $Q2D$, or three-dimensional $3D$ colloidal systems. Much less explored is the situation of two-dimensional, $2D$, or quasi-one-dimensional, $Q1D$, colloidal dispersions under soft confining potentials (23, 24) or when the colloids are explicitly embedded in a curved space or in a non-Euclidean geometry.

Generally speaking, confinement is a geometric concept that refers to limiting the particles to occupy a specific region in the space. As discussed above, it is possible to introduce a classification of the types of confinement, namely, hard, soft or a combination of them. These types of confinement depend on the geometric properties, such as dimension, length, area or volume associated to the confining geometric locus. However, there exists another type of confinement, limited to lines or surfaces, that is characterized by the local geometric properties such as the curvature(s) of the line or the surface. In fact, as discussed further below (§1.2,§5), colloidal dynamics will depend on the geometric nature of the type of confinement. Even more, the confinement may be dynamic itself, which can lead to many phenomena that still have to be studied in detail.

1.2. Non-Euclidean Geometry and Colloidal Soft Matter

One hallmark of colloids immersed in a host medium is their ability to diffuse (30). Diffusion is strongly affected by the geometry and symmetries of the space where the diffusive entities move (31). While differentiable manifolds have been the natural mathematical objects for describing the dynamics of space-time, in the last few decades, there has been a growing interest in this mathematical concept in problems arising in colloidal soft matter and biophysics (32, 33, 34).

From a theoretical point view, the description of diffusion in a curved space is still a challenging problem. Certain diffusion processes, however, can be modeled as transport phenomena on a curved differentiable manifold. For example, the diffusion of proteins on the cell membrane or the dynamics of biological motors along filaments can be considered as transport phenomena on a curved surface and on a curved line, respectively (35), although a continuous space is not always the best approach (36). Under certain approximations, curved differentiable manifolds arise as the emergent result of collective interactions between molecules that make up the material. For instance, interactions between amphiphilic molecules in an aqueous solution give rise to the formation of vesicles (37). Interfaces of soap, polymers, thin channels, and even $2D$ atomic materials, such as graphene, germanene, and silicene, can also spontaneously form curved surfaces. In fact, curved manifolds can also emerge by the disposition of the matter with the surroundings, such as the interface formed between immiscible liquids (38).

The inclusion of the geometry of the continuous medium on the diffusion of colloidal-like particles is a non-trivial task. Indeed, it represents a formidable physical and mathematical challenge (39, 40). A simple manner of approaching the stochastic motion of colloidal-like particles on a curve or a non-flat surface is through either a Langevin-type equation (41) or a Smoluchowski representation (42). As discussed further in §5, both schemes allow non-Euclidean geometry representation to be brought into the colloidal soft matter field, leading the possibility to explicitly study the effects of the geometry on the self-assembly and transport phenomena of colloids.

2. SELF-ASSEMBLY AND COLLOIDAL INTERACTIONS: CONFINEMENT IN EUCLIDEAN AND NON-EUCLIDEAN GEOMETRIES

2.1. Direct and indirect forces between colloids: the role of confinement

Colloids interact with each other via direct forces, such as excluded volume, electrostatic, and van der Waals (43, 44). The strength of the inter-particle interaction is of the order of k_BT and usually depends on the solution conditions, for instance, salt concentration, polymer concentration, pH, etc. (1). The direct forces depend on both the relative distance between colloids and the orientational degrees of freedom (if the potential is orientational dependent). Typically, the direct colloidal interactions are expressed as a function of the Euclidean distance and one assumes that they are not affected by confinement. However, there exist direct and effective wall-particle interactions that are a function of the geometrical features of the confining mechanisms (shape, topography, topology, and curvature), leading, for example, to the onset of structural transitions, see, e.g., Ref. (45) and references therein.

Due to the presence of the solvent, colloids exhibit special interactions that distinguish them from atoms: the hydrodynamic interactions (HI) (30). Contrary to (direct) particle-particle interactions, HI can be tuned, but never completely screened or switched off. In a simple physical picture, HI can be understood as follows. The motion of a given colloidal particle induces a flow field in the solvent, which is felt by the surrounding colloids, i.e., when a colloid moves, it displaces the fluid in its immediate vicinity (30). Thus, the motion of one colloidal particle causes a solvent-mediated force on the neighboring colloidal particles. HI lead to non-trivial hydrodynamic coupling among colloids that extends over many mean-interparticle distances (46). HI are hence mediated by the solvent and affected by the confinement of the colloids (47). Therefore, HI are a particular kind of indirect interactions. Although the effects of HI on the dynamical coupling between two colloids or a colloid near a wall have been the subjects of intense research during the last few decades (48), HI contributions to colloidal dynamics are far from being completely understood. The reason is partially related to the fact that colloidal dynamics extends over a wide range of temporal scales due to the enormous difference in size and mass between the colloids and the solvent molecules, and that under confinement, hydrodynamic interactions remain long-ranged, decaying algebraically with the inter-particle Euclidean distance, except for the case of confinement in a rigid linear channel, see, e.g., Ref. (47) and references therein. The understanding of the effects of HI under bulk and confinement conditions on the colloidal transport is also of relevance in other branches of science, such as biology, since phenomena like hydrodynamic synchronization in biological systems (sperm, cilia, flagella) (49, 50) and the dynamics of microswimmers (50, 51) can only be explained in terms of hydrodynamic coupling.

2.2. Colloidal phase behavior and free energy landscape of colloids under confinement

The equilibrium phase behavior of colloidal suspensions is determined by the delicate interplay between the (internal) energy, U, and entropy, S. In experiments, that interplay can be controlled by means of model colloidal systems (52). Both quantities define the free energy ($F = U - TS$ (53)) landscape accessible to the colloidal dispersion; this quantity describes the thermodynamic stability of the dispersion and is also the basis for the description of non-equilibrium processes (53).

Colloids can be arranged in multiple structural scenarios (§2.1) leading to a large diversity of colloidal phases even in bulk dispersions. Of course, richer and unexpected thermodynamic phases are seen when the colloids are geometrically or spatially confined. In this scenario, the free energy landscape accessible to colloids also becomes a function of the confinement, see, e.g., Ref. (54) and references therein. Then, the free energy landscape can be manipulated by confinement to control the colloidal self-assembly. For example, computer simulations and experiments of colloids interacting through short- and long-ranged repulsive potentials and confined on the surface of a sphere (54, 55), or along a circle (56) or an ellipse (57), have shown that the resulting self-assembly leads to very particular colloidal ordering, including aggregation and formation of colloidal clusters with specific orientational symmetries (54) and the transition between liquid-like states and crystal-like states (55) that correspond to local structures composed of "magic numbers". The term "magic number" is typically used in analogy with the formation of a stable atomic nucleus characterized by a certain number of nucleons necessary to form closed shells. In confined colloidal systems, the most stable clusters are those with a "magic number" of particles that allow the formation of closed shells that minimize the free energy (54).

Thus, controlling the self-assembly of colloidal particles into different microstructures, morphologies, and phases by manipulating the free energy landscape through the imposition of geometrical restrictions could provide the basis to fabricate hierarchically structured materials with nontrivial emergent properties (e.g., optical, electrical, magnetic, mechanical, thermal, and acoustic) of relevance for the design and development of new technologies.

3. COLLOIDS UNDER CONFINEMENT: HISTORICAL REVIEW

3.1. Equilibrium and non-equilibrium states

Hard-sphere or repulsive colloids of uniform size confined to a $2D$ plane, whether through sedimentation or walls to a thin layer (e.g., (74) or through trapping at the interface between two fluids (e.g., (58) Fig. 1(a)), form ordered crystals with hexatic symmetry. These crystals are not thermodynamically stable, however, because long-wavelength fluctuations (LWFs) representing acoustic phonons eventually disrupt the crystalline order (75).

Confining colloids on a $2D$ curved interface introduces geometric frustration that alters the particle organization. Generally, colloids can no longer pack in the simple triangular lattice found in $2D$. On a sphere with positive Gaussian curvature, the lattice includes defects to accommodate the spatial curvature (Fig. 1(b)). Additional defects form with increasing surface curvature; these are topologically charged disclinations arranged into high-angle grain boundaries that terminate within the crystal. On $2D$ surfaces with negative Gaussian curvature, the lattice accommodates the curvature by forming lines of dislocations

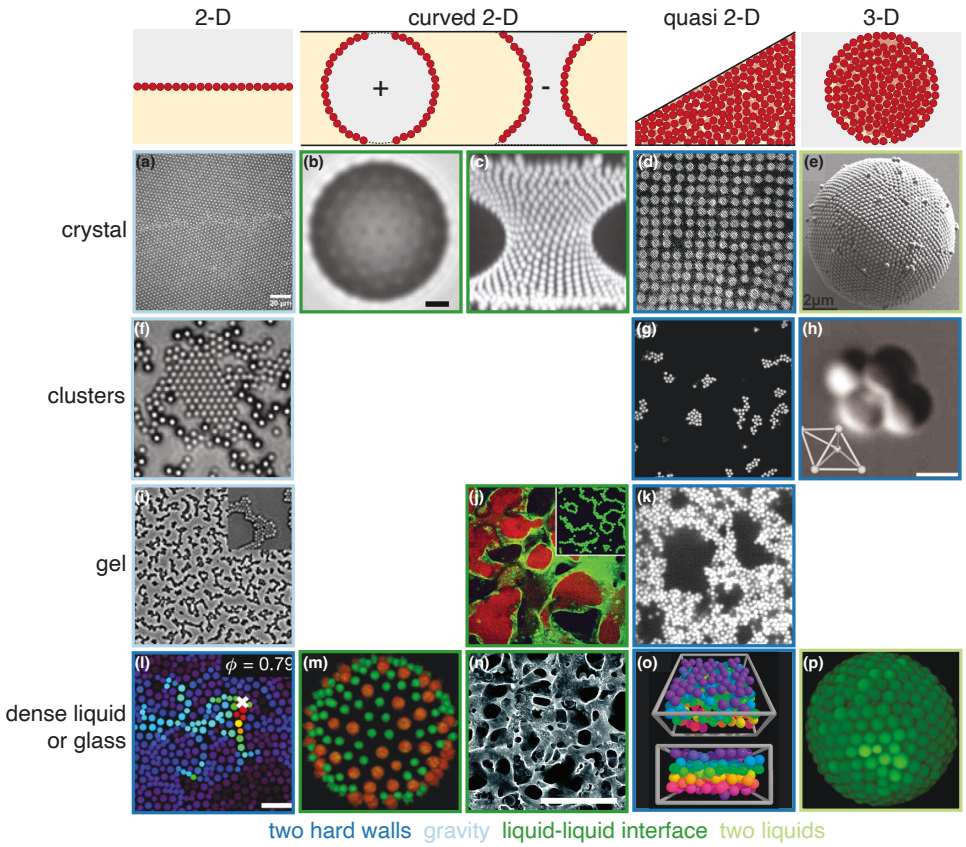

Figure 1

Images of confined colloidal suspensions with hard-sphere or isotropic attractive interactions across dimension and state behavior. (a – e) Crystals. (a) Reprinted figure with permission from Ref. (58). Copyright 2010 by the American Physical Society. (b) From Ref. (59). Reprinted with permission from AAAS. (c) Reproduced with permission from Ref. (60). (d) Reprinted figure with permission from Ref. (61). Copyright 1983 by the American Physical Society. (e) Reprinted from Ref. (62)). (f – h) Cluster phases. (f) Reproduced with permission from Ref. (63). (g) Reproduced from Ref. (64) with permission from the Royal Society of Chemistry. (h) From Ref. (65)). Reprinted with permission from AAAS. (i – k) Gels. (i) Reprinted from Ref. (66) under a CC-BY license (https://creativecommons.org/licenses/by/4.0/). (j) Reprinted figure with permission from Ref. (67). Copyright 2010 by the American Physical Society. (k) Reprinted figure with permission from Ref. (68)). Copyright 2012 by the American Physical Society. (l – p) Dense liquids or glasses. (l) Reproduced with permission from Ref. (69). (m) Reproduced from Ref. (70) under a CC-BY license (https://creativecommons.org/licenses/by/4.0/). (n) Reproduced from Ref. (71) with permission from the Royal Society of Chemistry. (o) Reprinted from Ref. (72), with the permission of AIP Publishing. (p) Reprinted figure with permission from Ref. (73)). Copyright 2016 by the American Physical Society. Border colors indicate the confinement mechanism.

without topological charge (Fig. 1(c)).(60)

Colloids confined in films whose thickness is less than approximately ten particle diameters can be considered quasi-two-dimensional. In equilibrium, confined hard-sphere or

repulsive colloids again form ordered phases, but whose structure depends on the commensurability of the colloid size and spacing. In quasi-2D thin films, colloids pack in alternating triangular ($\triangle$) and square ($\square$) planar lattices as the film thickness is increased (Fig. 1(d)) (61). Buckled phases can form in the $\triangle \rightarrow \square$ transition (76, 77) to maximize the local packing fraction (78). Thus, the unique close-packed crystal structure of hard spheres is lost when colloids are confined. Instead, many solids compete for the thermodynamically stable state (79), and the equilibrium phase diagram contains regions of liquid-solid coexistence (80). Finally, defective crystal-like states form when colloids are confined in 3D (Fig. 1(e)), with the most stable states corresponding to symmetries with closed shells.(54)

When an interparticle attraction is induced between the colloids (e.g., by adding a depletant polymer, using binary solvent mixtures, or altering the particle wettability), a variety of out-of-equilibrium phases can form. Colloids confined in 2D, quasi-2D, and 3D can all form clusters (Figs. 1)(f–h)). In 2D and quasi-2D, the local order of the cluster remains triangular (64). The structure of colloids confined in 3D within emulsion droplets depends on the interaction of the particles with the walls (81). These interactions dictate whether colloids form small clusters (Fig. 1(h)) or supraparticles (Fig. 1(e)).

Attractive colloids can form space-spanning colloidal gels when the attractions are sufficiently strong and/or the volume fraction is sufficiently high. Attractive suspensions that are fluid-like in bulk can form gels (Fig. 1(j)) when confined in quasi-2D (82, 68). Gelation is thought to arise from confined-driven changes in the strength of interactions between particles. Whereas neighboring walls are expected to enhance depletion through reduction of free volume, the depletion interactions are stronger than predicted from the classical Asakura-Oosawa model (83). These strengthened attractions have been attributed to solvent effects (83) or reductions in the electrostatic repulsion between particles due to nearby walls (84).

Finally, dense colloidal liquids can form out-of-equilibrium glasses when confined (Figs. 1(l – p). Confinement in quasi-2D wedges (85) or films (86) drives a transition from dense supercooled liquid to glass as the strength of confinement is increased. The nearby walls can induce layering (85, 87) or ordering (88) in dense suspensions, which in turn affects transport properties (§3.2). Because confinement can enhance the coupling of structure and dynamics, confining glasses in 2D (89) and 3D (73) provide a platform in which to test theories for the glass transition. Finally, colloids confined in porous media exhibit both localization and glass transitions, which are respectively determined by the medium structure and collective caging (90, 91).

Rigid boundaries induce structuring, and thus size-disperse mixtures are generally used in studies of dense confined suspensions to frustrate crystallization. Nonetheless, the commensurability of the average particle size and slit width affects local bond order (92) and leads to multiple re-entrant glass transitions (93) even in highly disperse mixtures.

3.2. Transport phenomena

The coupling between structure and confinement modifies the transport properties of confined colloids. The mean-square displacement of colloids confined in a quasi-1D narrow channel scales as $t^{1/2}$ as predicted for single-file diffusion (SFD) (94, 95), to be further discussed in (§5.3). This scaling arises because geometric confinement restricts the motion of the particles and hinders large displacements (96). Hydrodynamic interactions in quasi-1D strongly affect transport: whereas HI between diffusing particles are screened (97), HI

between particles and walls leads to oscillations in the relative pair diffusion coefficient (98). In binary suspensions, however, hydrodynamic flows from particles of different sizes interfere to suppress these oscillations (99).

Interactions with nearby walls also introduce confinement effects on transport in $2D$ and $3D$. Near a wall, diffusion of isolated colloids is slowed due to the hydrodynamic drag imposed by the walls (100, 101). HI with the walls also dictate slowing of particles diffusing in disordered (102) and ordered (103) porous media. In concentrated fluid suspensions confined in $2D$, long-range, dipolar interactions induced by the flow field of a diffusing particle lead to anomalous transport (104).

Confinement modifies transport properties in colloidal supercooled liquids and glasses, where particles relax cooperatively. First, confinement leads to strong slowing of dynamics. In quasi-$2D$-confinement, the dynamics of dense colloidal liquids confined in thin wedges (85) or films (86) slow dramatically as the confining thickness is decreased. Motion perpendicular to and near the walls is most hindered (85, 87), suggesting that interactions with the walls contribute to slowing.

Confinement also induces changes in the shape and size of the cooperatively relaxing regions (CRRs). In planar $2D$ confinement, local CRR domains become increasingly rigid as the particle concentration is increased to induce caging (69). In quasi-$2D$ confinement, the size of CRRs scales similarly with the relaxation time scale, suggesting that the confinement length scale sets the size of relaxations (105). On curved $2D$ surfaces, the shape of CRRs changes from fractal to compact upon increasing particle density (70).

Finally, the dynamics of confined glassy suspensions may be affected by the LWFs that destabilize colloidal crystals in $2D$. In planar $2D$ (106, 107) and quasi-$2D$ (108) confinements, LWFs are present and provide an additional avenue for particle motion. While LWFs persist across the crossover from $2D$ to quasi-$2D$, their magnitude depends non-monotonically on the confinement thickness due to the competition between caging and dimensionality (109). Intriguingly, LWFs are not present when colloids are confined on the surface of a strongly curved sphere whose radius is of order four particle diameters (70).

4. NON-VIBRATING GRANULAR MATTER AS MODEL SYSTEM TO STUDY COLLOIDS UNDER CONFINEMENT

The study of a colloidal dispersion at the particle level remains challenging at very short times, i.e., in the ballistic regime, due to the spatial (angstrom scale) and temporal (nanosecond scale) resolutions required to fully describe it (110); tracking of every particle in a colloidal dispersion with multiple time and length scales is not trivial, even though novel experimental techniques have recently been developed (110, 111, 112, 113). As an alternate approach, macroscopic systems with experimentally accessible scales, i.e., grain-based models, have been developed for direct observation to shed light on the behavior of colloidal dispersions. Although the size of the grains differs from the colloidal dimension by several orders of magnitude, and the interaction between grains is highly dissipative, which can lead to very complex non-equilibrium phenomena, in this review, we simply focus on granular systems as well controlled experimental models that allow us to capture the phenomenology of colloids.

In particular, fluidized millimeter-sized particle systems have proven to be very useful models of both colloidal and molecular fluids. Mathematically speaking, the description of the particle motion is similar to that for colloids with the advantage that the temporal ($\sim$

milliseconds) and spatial ($\sim$ millimeters) scales are experimentally accessible, for example, to standard video microscopy techniques. Although these macroscopic systems are driven, athermal, and clearly out of equilibrium, they have been successfully used under stationary conditions to study certain aspects of supercooled liquids, bubbles, and colloidal dispersions (114, 115, 116, 117).

4.1. Fluidization mechanism and effective temperature

Vibration, shaking, and shearing are the most common mechanisms to inject energy and hence fluidize a granular system. Features such as the growth of viscosity, multiple step relaxation times, fragility, dynamical heterogeneity, aging, crystallization, and amorphous solidification have been studied with granular systems by varying the particle concentration and mechanism of fluidization (116, 118). The self-organization of proteins and macromolecules within cells are found to behave as granular matter (119); the self-assembly and dynamics of cells follow the same physical laws as shaken granular materials (120).

The study of crystallization in colloids and molecular systems has been addressed by using granular systems by fluidizing them through oscillating shear forces, electric or magnetic fields (121, 122, 123). In granular systems, time-varying fields have been used to successfully exploit self-assembly (124, 125, 126). Rotating magnetic fields have been manipulated to assemble dissipative structures, such as magnetic "spinners" (123, 127), non-magnetic particles immersed in a magnetic fluid, (128) and steel balls (126). In vibrated-sheared granular spheres, competing disordering and crystallizing processes have been reported, which differ from those found when vibrated or sheared was performed separately (129). During the shearing cycles in granular spheres immersed in a liquid, nuclei emerge, grow, and shrink (125), leading to a structural transition from a disordered loose packing to a symmetric densely packed.

The methods of fluidization can be classified as vibrating and nonvibrating. In vibrating systems, the experimental setups have moving parts. In contrast, nonvibrating granular matter systems, i.e., air-driven, magnetic-driven, and levitating-driven (130, 126, 131), do not require moving parts in the experimental setup.

Nonvibrating two-dimensional granular systems using an alternating magnetic field to externally excite motion accurately mimic passive and active colloids (132, 133, 134); the interaction between granular beads can be controlled via the magnitude of the magnetic field and the concentration of beads. The magnetic field has the general form $B = B_c + B_o \sin 2\pi f t$, with B_c being a constant field (133) and B_o the amplitude of the alternating contribution of the field. The effective temperature is proportional to B_o. This system experiences a Brownian-like motion, and despite being highly dissipative, it reaches a stationary state due to the continuous injection of energy from the alternating magnetic field. Its behavior exhibits the characteristics that define an Ornstein-Uhlenbeck process, allowing the use of tools developed for colloids in thermal equilibrium (132). Lowering the effective temperature results in different dynamics and, consequently, a plethora of structural rearrangements.

Studies of solidification using the non-vibrating granular model (133, 134) reproduce essential features of non-equilibrium transitions in colloids. At high temperatures, the particles move quickly and randomly on the surface. The motion slows upon lowering the effective temperature, causing repulsive interactions to become important, and defining an average separation between particles. When a temperature quench is applied, the diffusion

coefficient starts to decrease very quickly until the temperature reaches values lower than a threshold value below which its rate of decrease becomes slower. The intersection of both temperature regimes defines the so-called glass transition temperature T_g. Above T_g, the particles diffuse as in a fluid as shown by the particle trajectories in the right image of Fig. 2(a), whereas below T_g the trajectories are confined as in a solid, as shown in the left image of Fig. 2(a).

By determining the diffusion coefficient of the granular particles, it is possible to define an effective viscosity and, therefore, to obtain Angell-like plots. The relation between the fragility index m and the regularity factor α demonstrated that a strong glass former is more ordered than a fragile one (134). This result made explicit the versatility of the non-vibrating granular system to model glass transitions.

4.2. Soft confinement

In a nonvibrating granular system, soft confinement is imposed when the particles are settled on a concave surface, which models a harmonic well that restricts the area available to the beads. The soft potential can be tuned by varying the surface's concaveness, i.e., the curvature magnitude, driving the system to different degrees of ordering. The results shed light on crystallization in colloidal and molecular systems (135). Recent theoretical and experimental studies confirmed that the nucleation process occurs in at least two steps: an amorphous aggregate forms by overcoming a first free energy energy and, subsequently, forms an ordered nucleus by overcoming a second barrier, in contrast to the classical theory of nucleation (136). In this context, granular systems have allowed us to unravel the nature of this process. However, recent experiments in colloidal systems have reported multi-step nucleation processes (137, 138, 139). In particular, one-step nucleation in quasi-2D colloidal systems with particles interacting with a competing potential (64) suggests that the type of interaction may determine the resulting nucleation process. Then, further experiments and theoretical models (using different interparticle potentials) would be necessary to better understand the conditions at which colloids nucleate in one or several steps.

In Refs. 126, 140, the formation of glassy, crystalline, and mixed states using a nonvibrating granular system with soft confinement has been reported. The experiments started at a high temperature, which dropped at various cooling rates until the system achieved an arrested state (126). If the cooling is fast, the particles do not have enough time to find and remain at their energy minimum, forming amorphous or glassy structures, Fig. 2(d). When an intermediate cooling rate is used, mixed arrangements can be obtained between ordered aggregates and amorphous zones, Fig. 2(d). If the cooling is slow enough, the probability that the particles reach their minimum energy position is higher, and the particles can form crystalline arrangements, Fig. 2(d).

When the system crystallizes, the initial formation of the nucleus was studied in detail (126, 135). These studies on the birth of the crystal nucleus and subsequent crystal growth support the non-classical theory of two steps, where initially a dense amorphous aggregate of particles is formed. Then, in the second stage, this aggregate undergoes internal rearrangements to form the crystalline nucleus. As the aggregate grows, the crystal inside also grows until it reaches a certain size, after which it continues its growth according to classical crystal growth theory.

In a series of experiments at different concaveness, the two-step features of the crystallization process were more evident as the depth of the parabolic potential increases; the

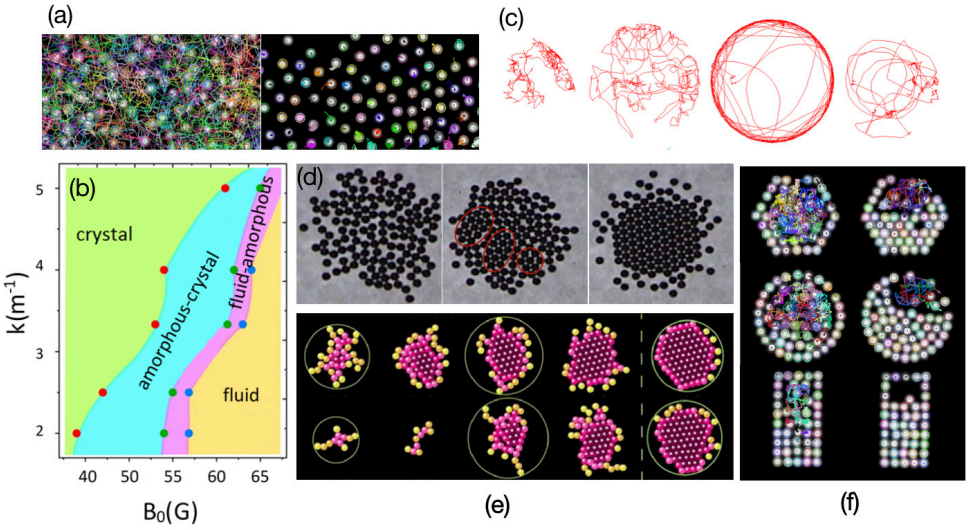

Figure 2

(a) Trajectories of granular beads with diffusive motion when the effective temperature is above (left) and below (right) the glass transition temperature. (b) State diagram of a nonvibrating granular system in terms of the magnetic field B, which acts as an effective temperature, and the curvature of the lens k, which acts as an effective pressure. (c) Trajectories of a single granular bead for various field frequencies. The particle undergoes Brownian-like motion at low frequencies that becomes persistent at higher frequencies. After a threshold frequency, each trajectory becomes Brownian-like again until it becomes self-trapped around a point for even higher frequencies. (d) Different final configurations of a granular system that cools at three different speeds; the configuration on the left corresponds to the fastest cooling, and the one on the right corresponds to the slowest. The configuration formed by an intermediate cooling rate presents small regions where the particles form hexagonal closed-packed structures. (e) Growth of an aggregate at different effective temperatures using two lenses of different curvature. The comparison is carried out at the same temperature except for the aggregate corresponding to the final structure. The time of the crystallization process depends on the curvature of the lenses. (f) Structures formed by three different confinements. The configurations on the left correspond to linear cooling, and the column on the right to stepwise cooling. (a), (c) and (f) are cases associated with rigid confinement, and (b), (d) and (e) with soft confinement.

nucleus size is larger for deeper concaveness of the parabolic potential, Fig. 2(e). If the depth of the parabolic potential exceeded a certain value, however, the reordering process of the second step did not occur. Figure 2(b) (135) shows a phase diagram where fluid, co-existing, and crystalline regions were observed for different values of concavities and magnetic field magnitudes.

4.3. Rigid confinement

Fig. 2(f) shows the strong effects of rigid confinement on crystallization in nonvibrating granular systems in three different geometries: hexagonal, circular, and rectangular. Confinement reduces the crystallization time compared to the bulk case, i.e., there is no rigid confinement. In a hexagonal cell the closed hexagonal arrangement is favored, the rectangular cell imposes square order, and the circular cell favors the formation of necklace-like structures piled one over the other. As the particles move away from the walls, the influence of the container shape decreases, and the tendency to form an ordered hexagonal closed arrangement increases.

The dynamics of a single granular magnetized particle (a model active particle) in rigid confinement, i.e., a quasi-one-dimensional circular rail, was studied (141). A dynamical transition between a diffusive and highly persistent magnetic motion was observed by varying the magnetic moment. The limiting motion behaviors correspond to Brownian motion on the circle and a simple uniform circular motion, respectively. Furthermore, the smaller the magnetization of a particle, the larger the persistence length. At a fixed magnetic field, the motion transitions from diffusive to superdiffusive as the frequency increases, approaching a threshold where the persistence reaches its maximum. After this threshold, the motion becomes subdiffusive, and subsequently, at higher frequencies, the particle remains vibrating around a point (Fig. 2(c)).

5. COLLOIDAL PARTICLE DYNAMICS ON CURVED SPACES

5.1. Theoretical summary of a Brownian particle on curved spaces

In §3 and §4 we summarized several situations where colloids are constrained geometrically to surfaces and where colloids form surfaces by different mechanisms, illustrated in Figures 1 and 2. These material shapes or geometrical constraints where colloids move can be approximately represented by two classes of differentiable manifolds corresponding to regular curves, i.e., $1D$ manifolds, and regular surfaces, i.e., $2D$ manifolds, embedded in a $3D$ Euclidean space. A curve is characterized by its length L, curvature $\kappa(s)$, and torsion $\tau(s)$ (142), where s is the arc-length. In the case of a surface, the metric tensor $g_{ab}(x)$ and the extrinsic curvature tensor $K_{ab}(x)$, for $a = 1, 2$, are key quantities associated to the surface Σ; here $\{x^a\}$ are coordinates in each local patch (34). The curvatures (and torsion in the case of curves) not only characterize the geometry of the material but also represent external fields defined at each point in the manifold $\mathbb{M}$, which affect particle transport processes, see, e.g., Ref. (143) and references therein. In the following, we summarize the main results for the transport behavior of a single (passive or active) particle confined to a planar curve and a curved surface.

For a single particle confined to a planar curve or a curved surface, one can formulate proper Langevin-type equations (144). The overdamped limit, $t \gg M/\zeta$, where ζ and M denote the solvent friction and the mass of the colloid, respectively, can be achieved by ignoring the inertial terms in each Langevin equation (40). Using standard methods (145), one can show that the corresponding Fokker-Planck equations of these stochastic equations, in the Stratonovich sense, are given by the so-called Smoluchowski or diffusion equation on the corresponding manifold, that is,

$$\frac{\partial P}{\partial t} = D\Delta_{\mathbb{M}} P, \qquad 1.$$

where $D = k_B T/\zeta$ is the diffusion coefficient, $k_B T$ is the thermal energy, and $P(x,t)$ is the single particle probability density function. The operator $\Delta_{\mathbb{M}}$ is the Laplace-Beltrami operator acting on scalars associated to the manifold $\mathbb{M}$. In case of a curve, $\mathbb{M} = \boldsymbol{\gamma}$, the Laplace-Beltrami operator is $\Delta_{\boldsymbol{\gamma}} = \partial^2/\partial s^2$, whereas for a surface, $\mathbb{M} = \Sigma$, the operator is $\Delta_\Sigma = \frac{1}{\sqrt{g}}\partial_a \sqrt{g} g^{ab} \partial_b$, where g^{ab} are the components of the inverse metric tensor and g is the determinant of the metric tensor. It is clear how the diffusion processes of a single Brownian particle on the manifold depend on the geometry of the manifold; essentially, the Laplace-Beltrami operator has the geometrical content affecting the transport process of a single Brownian particle on $\mathbb{M}$.

The expectation values of certain observables can be used to study the quantitative contribution resulting from the geometry of $\mathbb{M}$. Commonly, the geodesic distance δs is used as a displacement of the particle (32), but also the Euclidean displacement $\delta \mathbf{R}$ defined as the Euclidean distance between two points on $\mathbb{M}$ can be a good observable to detect the curvature effects (41). Both observables can be used to probe the geometry of the manifold. For instance, for a compact $1D$ manifold without boundaries, it is remarkable that the mean-square arc-length displacement (MSAD) can be written for any closed curved of length L by $\left\langle [\delta s\,(t)]^2 \right\rangle = L^2 f(Dt/L^2)$ for a certain function $f(x)$ that can be given by an exact series (144). This MSAD has asymptotic behaviors at different time scales. At short times, $t \ll L^2/D$, it goes as $\left\langle [\delta s\,(t)]^2 \right\rangle \sim 2Dt$, and at long times, $t \gg L^2/D$, it behaves as $\left\langle [\delta s\,(t)]^2 \right\rangle \sim L^2/12$ (144). Both limits are consistent with the behavior examined by computer simulations and experiments of super-paramagnetic colloids confined in a circle (146). In addition, for any curved surface Σ, the mean-square geodesic displacement (MSGD) at the short-time regime can be given by the power series expansion $\left\langle [\delta s\,(t)]^2 \right\rangle \approx 4Dt - \sum_{n=2} G_n [K_G(x_0)](Dt)^n$, whose first coefficients G_n, with $n = 2, 3$, are explicitly known in terms of the Gaussian curvature $K_G(x)$ evaluated at the initial point $x = x_0$ of the motion of the particle, accounting for the curvature effects on the transport phenomena of the single colloid (32). Similarly, the mean-square Euclidean displacement $\left\langle [\delta \mathbf{R}(t)]^2 \right\rangle$ can measure curvature effects, but in this case, the measure depends exclusively on the extrinsic tensor $K_{ab}(x)$ (41).

In the long-time regime, the expectation value of any observable $\mathcal{O}(x)$ has the general behavior $\langle \mathcal{O}(x(t)) \rangle_{\mathbb{M}} \simeq \sigma_0 + \delta\sigma(\sqrt{Dt}/\ell)$, where a characteristic length ℓ associated to the size of the manifold, $\delta\sigma(x) = e^{-x^2}$ is an exponentially suppressed term, and $\sigma_0 = \mathrm{Vol}(\mathbb{M})^{-1} \int d^d x \sqrt{g}\ \mathcal{O}(x)$ is a constant, where $\mathrm{Vol}(\mathbb{M})$ is the volume of the manifold; further details can be found in (41). Both short- and long-time behaviors of the mean-square geodesic and Euclidean displacements have been verified using finite element methods in particular surfaces (143). These findings illustrate the difference between the mean-square geodesic and Euclidean displacement compared to their flat counterparts. This difference shows the role played by the curvature on the diffusion process at short times, well captured by local terms that do not change under general coordinate transformations. In contrast, at the long-time regime, the behavior of the expectation value of any observable is a global expression that depends exclusively on the metric tensor.

The covariant approach can also be implemented to study active colloid motion on curved manifolds (141, 147, 148). The motion of a $1D$ run-and-tumble active particle in a circle can be described by two parameters: the constant average particle velocity, v_0, and the uniform tumbling frequency rate, λ. The persistence time is defined as $\tau_c = \lambda^{-1}$, the average time the particle takes to tumble. The persistence length is $\ell_c = v_0 \tau_c$, representing the average distance traveled by the particle during the persistence time. In particular,

it can be shown that the MSAD can be written for any closed curved of length L by $\left\langle [\delta s\,(t)]^2 \right\rangle = L^2 f_a(D_{\text{eff}} t/L^2, \ell_c/L)$, where $D_{\text{eff}} := v_0^2 \tau_c$ is an effective diffusion coefficient and $f_a(x, y)$ is a certain function that can be given by an exact series (141). The "run-and-tumble" model developed in (141) predicted that there are two states of motion on a circle: an erratic motion (disordered phase for $\ell_c < L/4\pi$) and a persistent motion (ordered phase for $\ell_c > L/4\pi$). In addition, when $\ell_c \gg L/2\pi$, the particle moves in a uniform circle, whereas when $\ell_c \ll L/2\pi$, it follows the usual Brownian motion on the circle, while the diffusion coefficient D is identified with D_{eff}. In addition, (141) analyzed the transition by examining the stochastic behavior of a magnetized granular particle. The particle was confined to a quasi-1D circular channel and was activated by an alternating magnetic field acting as a reservoir, as described in §4.1.

The stochastic motion of active Brownian particles on a curved surface (147) can also be described by MSGD, which captures the relationship between the Gaussian curvature and the activity of the colloid. Using this approach, the dynamics of an active Brownian particle on a spherical surface was found to exhibit a dynamical phase transition between an oscillatory behavior and a monotonic one within the random behavior of the active particle (147, 148), which is a dynamical transition of the same class as the run-and-tumble particle on the circle.

5.2. Theoretical summary for many-particles Brownian particles: the covariant colloidal dynamics approach

A generalized Ermack-McCammon algorithm was developed to study a broader class of transport phenomena in heterogeneous environments (144), for example, the trapping of colloids in regions of greatest curvature (57, 149). From this approach, it was possible to derive a covariant Smoluchowski equation of N diffusing particles in curved spaces (42), including the intermolecular forces $\mathbf{F}_{ij}$ defined in the Euclidean space where the manifold $\mathbb{M}$ is embedded. In particular, Eq. (1) for a single Brownian particle can be generalized to the situation where the Brownian particles interact not only due to the intermolecular potentials (144), but also due to geometrical mechanisms originating from the curvature,

$$\partial_t p = D_0 \sum_{i=1}^{N} \Delta_{\mathbb{M},i} p - \frac{1}{\zeta} \sum_{i=1}^{N} \sum_{j \neq i}^{N} \nabla_{\alpha,i} \left(F_{ij}^{\alpha} p \right), \tag{2.}$$

where $p = p(x_1, ..., x_N, t)$ is the joint probability density of the colloidal particles, ζ and $D_0 = k_B T/\zeta$ are the friction and collective diffusion coefficients, respectively, $F_{ij}^{\alpha} = \mathbf{e}^{\alpha}(x_i) \cdot \mathbf{F}_{ij}(x_i, x_j)$ is the projection over the tangent space of $\mathbb{M}$ of the force experienced by the $i-$th particle due to the $j-$th particle and $\Delta_{\mathbb{M},i}$ and $\nabla_{\alpha,i}$ are the Laplace-Beltrami operator and the covariant derivative, respectively, both acting on the coordinates of the $i-$th particle. All the geometric information of the system is contained in the differential operators and the interaction terms. From this approach, the MSGD for a tagged particle in the short-time regime is given by,

$$\begin{aligned} \left\langle [\delta s\,(t)]^2 \right\rangle \;=\; 4Dt - \Bigg[& \frac{4}{3N} \sum_{i=1}^{N} K_G(x_i) \\ & - \frac{2}{N k_B T} \sum_{i,j}^{N} \left(\mathbf{e}^{\alpha}(x_i) \cdot \partial_{\alpha,i} \mathbf{F}_{ij}(x_i, x_j) - K(x_i) \mathbf{N}(x_i) \cdot \mathbf{F}_{ij}(x_i, x_j) \right) \Bigg] (Dt)^2 + \cdots, \end{aligned} \tag{3.}$$

where the geometrical information is associated with the value of the Gaussian curvature $K_G(x)$, the mean curvature $K(x)$, the tangent vector $\mathbf{e}^{\alpha}(x)$ and the normal vector $\mathbf{N}(x)$ evaluated at the positions of the particles (42).

The intermolecular forces $\mathbf{F}_{ij}$ are usually derived from a potential such that $\mathbf{F}_{ij} = -\nabla_{\mathbf{r}_i} V(|\mathbf{r}_i - \mathbf{r}_j|)$, where $\nabla_{\mathbf{r}_i}$ is the usual Euclidean gradient. Now, the condition $\mathbf{r}_i = \mathbf{X}(x_i)$ is imposed since particles are holonomically constrained to the manifold, where $\mathbf{X}(x_i)$ is the parameterization of the manifold. Since in Eq. 2 only tangent forces are involved, one has $F_{ij}^{\alpha} = -\nabla_i^{\alpha}\Phi(x_i, x_j)$ (see (42) for the details), where the symmetric potential $\Phi(x_i, x_j) \equiv V(|\mathbf{X}(x_i) - \mathbf{X}(x_j)|)$ is identified.

Taking into account the marginal probability densities, one can integrate the Smoluchowski equation (Eq. 2) over the degrees of freedom corresponding to the $N-1$ particles. The same procedure in Euclidean space (30) can be straightforwardly implemented in the curved case, except that one has to consider the Stokes theorem on the manifold and appropriate boundary conditions (150). The integrated Smoluchowski equation for the one-body probability distribution $\rho(x,t)$ in curved space is

$$\partial_t \rho(x,t) = D_0 \Delta_{\mathbb{M}} \rho(x,t) + \frac{(N-1)}{N\zeta} \nabla_{\alpha} \left[\rho(x,t) \int \nabla^{\alpha} \Phi(x,x') \rho(x',t) \mathcal{G}(x,x',t) \sqrt{g(x')} d^d x' \right], \quad 4.$$

where $\mathcal{G}(x,x',t)$ is the van Hove function in curved space (150). The factor $(N-1)/N$ indicates that in a closed manifold, one can have a certain number of particles, i.e., a finite-size system; see, e.g., (Fig. 1(m)) (70). In the last expression, the first term in the right-hand side is an entropic contribution due to the collective effect of the solvent. The second term is an energetic contribution, depending on the interaction potential. If one sets $\Phi = 0$, one immediately recovers the Smoluchowski equation for a free particle in a manifold (32). Furthermore, the geometrical effects are considered in the differential operators and in the factors that involve the metric tensor and its determinant, which now are clearly mixed with the interaction term. The above equation recovers the Euclidean approach of the Smoluchowski equation (30) for particles in an Euclidean space. Notably, Eq. 4 is a novel and original result that will be the starting point to analyze different dynamical phenomena in colloidal systems constrained to move on a curved manifold, such as the ones described in §3.2.

Furthermore, the covariant form of the Smoluchowski equation, either Eq. 2 or Eq. 4, opens up the possibility of developing a theoretical framework to study phenomena that cannot be understood with the standard Statistical Mechanics approximations based on a Euclidean formulation. For example, the onset of spinodal decomposition in colloidal dispersions where the particles interact with short-ranged attractive forces and constrained to a curved space (e.g., the bijels in Fig. 1j). In addition, the covariant formalism can be straightforwardly employed to highlight the role of the geometry on the equilibrium equation of the state of colloidal dispersions embedded in a curved space, to elucidate the geometrical contributions during the onset of non-equilibrium states, to study the particle dynamics on manifolds and to investigate the curvature affects on the structural, kinetic and phase transitions of passive and active colloids, among other examples.

Two aspects that need to be considered to extend the covariant description of the Smoluchowski equation are the generalization of the fluctuation-dissipation theorem and the inclusion of the hydrodynamic interactions in the manifold. Both aspects are crucial to account for the dynamical properties on the manifold, since they are intimately related

to the onset of non-equilibrium states. Furthermore, this theoretical framework can be extended to include rotational motion on the manifold to consider anisotropic particles, such as rods (151), or physical scenarios in which the anisotropy is associated with the particle interaction, like in patchy colloids (152, 153, 154).

5.3. Time scales and transition times: the role of the geometry

The generalization of the Ermak-McCammon algorithm to carry out Brownian dynamics simulations in non-Euclidean spaces (144) described in §5.2 was used to explore the dynamics of interacting colloids moving on a circle, S^1, and a sphere, S^2. The resulting dynamics made evident the rich scenario that emerges when particles move in curved spaces. In particular, different time scales and temporal regimes, which can be explained in terms of the interparticle interaction, system size and geometry, were explicitly delineated (144).

To validate the preliminary simulation results for the case of N interacting colloids on a circle of radius R, video microscopy experiments with paramagnetic colloids confined to lithographic circular channels (whose radius is larger than the particle size) subjected to an external magnetic field were performed and extensive Brownian dynamics simulations were carried out (146). The colloid dynamics was characterized via the MSAD, $\langle[\delta s(t)]^2\rangle$, where the arc length δs is related to the angular displacement, $\delta\phi(t)$, via $\delta s(t) = R\delta\phi(t)$. This colloidal model system displayed four temporal regimes: 1) one-dimensional free diffusion at short times, $\langle[\delta s(t)]^2\rangle \sim t$; 2) SFD (discussed in §3.2), $\langle[\delta s(t)]^2\rangle \sim \sqrt{t}$; 3) free-cluster rotational diffusion, $\langle[\delta s(t)]^2\rangle \sim t/N$; and 4) the expected saturation due to the confinement, $\langle[\delta s(t)]^2\rangle = L^2/12$, where L is the perimeter of the circle (144, 146).

Analytical expressions for $\langle[\delta s(t)]^2\rangle$ and the transition times, i.e., the time between two consecutive temporal regimes, obtained from scaling arguments, accurately reproduced both experiments and simulations (146). The first transition time, τ_d, described the transition from normal diffusion to subdiffusion, basically when the mutual passage restriction starts to be dominant; here the interplay between the confinement and the interparticle potential played a major role, defining the subdiffusive behavior characteristic of SFD. The second transition time, τ_c, represented the transition from SFD to again normal diffusion, i.e., MSAD $\sim t$. In that temporal regime, however, the particles have acquired an effective diffusion coefficient given by the free particle diffusion divided by the total number of particles, N; here the finite size effects control the particle dynamical behavior. Finally, the third transition time, τ_G, signaled the transition from the free-cluster dynamics to the so-called geometrical time regime, where the particles have fully explored their available phase space and, therefore, the dynamics depends exclusively on the geometrical properties of the manifold where the particles are embedded.

Thus, the characterization of the time scales and the transition times experienced by the particles revealed that colloidal transport under confinement conditions depends non-trivially on the interplay between the interparticle potential, the intrinsic geometrical features of the space, and the finite size of the system.

6. SUMMARY AND PERSPECTIVES

In this review, we provide an overview of the effects of the geometry and confinement on self-assembly and transport phenomena of colloids. We highlighted typical features of colloidal suspensions and introduced a distinction between confinement and geometry to establish

a clear difference between both mechanisms that can lead to novel colloidal phenomena. Later, we briefly discussed how the geometrical properties of the space affect the free energy landscape and, in consequence, the colloidal phase behavior. We also summarized historical studies probing the effects of confinement on both the equilibrium and non-equilibrium thermodynamic states and on colloidal transport. We reviewed how granular matter can be used as an ideal model system to explore in detail the effects of confinement in colloidal matter. As the persistence of the motion is readily controlled by the frequency and the magnetic field, this system can be used to model the self-assembly and phase transition of active and passive colloids under several confinement conditions in experiments. Finally, we revisited the physical and mathematical bases to build a covariant description of the colloid dynamics in curved spaces.

Last but not least, we emphasize that additional experiments with model active and passive systems, such as the granular system here discussed, are needed to explore in more detail the role of the geometry on both the self-assembly and transport of colloids and to test the predictions of the covariant formulation. In fact, the limiting cases of equations 2 and 4 will also serve as a benchmark to computational, molecular simulation schemes and even novel experimental setups adapted to study the behavior of colloids in non-Euclidean spaces and under complex confinement conditions.

DISCLOSURE STATEMENT

The authors are not aware of any affiliations, memberships, funding, or financial holdings that might be perceived as affecting the objectivity of this review.

ACKNOWLEDGMENTS

R.E.M. and F.D. acknowledge financial support from Conahcyt (Grant No. 731759). J.C.C. is supported by the National Science Foundation (DMR-1904531) and the Welch Foundation (E-1869). R.C.-P. acknowledges financial support from Conahcyt (Grant No. CBF2023-2024-3350), the Marcos Moshinsky fellowship, and the University of Guanajuato (CIIC 093/2024). This scientific contribution is dedicated to the memory of Prof. Stefan U. Egelhaaf (RIP).

LITERATURE CITED

1. Hunter RJ. 2001. Foundations of colloid science. Oxford University Press
2. Conrad JC, Ferreira SR, Yoshikawa J, Shepherd RF, Ahn BY, Lewis JA. 2011. *Curr. Opin. Colloid Interface Sci.* 16(1):71–79
3. Zhu C, Pascall AJ, Dudukovic N, Worsley MA, Kuntz JD, et al. 2019. *Annu. Rev. Chem. Biomol. Eng.* 10(1):17–42PMID: 30951639
4. Mewis J, Wagner NJ. 2012. Colloidal suspension rheology. Cambridge University Press
5. Dagdug L, Peña J, Pompa-García I. 2024. Diffusion under confinement, a journey through counterintuition. Springer
6. Zöttl A, Stark H. 2023. *Annu. Rev. Condens. Matter Phys.* 14(1):109–127
7. Zaccarelli E. 2007. *J. Phys. Condens. Matter* 19(32):323101
8. Glansdorff P, Prigogine I. 1971. Thermodynamic theory of structure, stability and fluctuations. Wiley-Interscience
9. Vicsek T, Zafeiris A. 2012. *Phys. Rep.* 517(3):71–140

10. Bechinger C, Di Leonardo R, Löwen H, Reichhardt C, Volpe G, Volpe G. 2016. *Rev. Mod. Phys.* 88(4):045006
11. Ramírez-González P, Medina-Noyola M. 2010. *Phys. Rev. E* 82(6):061504
12. Alarcon F, Valeriani C, Pagonabarraga I. 2017. *Soft Matter* 13(4):814–826
13. Martinez R, Alarcon F, Rodriguez DR, Aragones JL, Valeriani C. 2018. *Eur. Phys. J. E* 41(8):91
14. Rogel Rodriguez D, Alarcon F, Martinez R, Ramírez J, Valeriani C. 2020. *Soft Matter* 16(5):1162–1169
15. Sevilla FJ. 2016. *Phys. Rev. E* 94(6):062120
16. Sevilla FJ, Rodríguez RF, Gomez-Solano JR. 2019. *Phys. Rev. E* 100(3):032123
17. Williams I, Oğuz EC, Bartlett P, Löwen H, Royall CP. 2013. *Nature Commun.* 4:2555
18. Rice SA. 2009. *Chem. Phys. Lett.* 479:1–13
19. Chaudhuri D, Sengupta S. 2008. *J. Chem. Phys.* 128:194702
20. Ricci A, Nielaba P, Sengupta S, Binder K. 2006. *Phys. Rev. E* 74:010404(R)
21. Curk T, de Hoogh A, Martinez-Veracoechea FJ, Eiser E, Frenkel D, et al. 2012. *Phys. Rev. E* 85:021502
22. Oğuz EC, Reinmüller A, Schöpe HJ, Palberg T, Messina R, Löwen H. 2012. *J. Phys.: Condens. Matter* 24:464123
23. Galván-Moya JE, Misko VR, Peeters FM. 2014. *Phys. Rev. B* 90:094111
24. Piacente G, Schweigert IV, Betouras JJ, Peeters FM. 2004. *Phys. Rev. B* 69:045324
25. Williams I, Oğuz EC, Bartlett P, Löwen H, Royall CP. 2015. *J. Chem. Phys.* 142:024505
26. Debabrata D, Winkler A, Yamani MH, Oettel M, Virnau P, Binder K. 2011. *J. Chem. Phys.* 134:214706
27. Herrera-Velarde S, Euán-Díaz EC, Castañeda-Priego R. 2021. *Colloids Interfaces* 5(2)
28. Williams I, Oğuz EC, Jack RL, Bartlett P, Löwen H, Royall CP. 2014. *J. Chem. Phys.* 140:104907
29. Evers F, Hanes RDL, Zunke C, Capellmann RF, Bewerunge J, et al. 2013. *Eur. Phys. J. Spec. Top.* 222:2995
30. Dhont JK. 1996. An introduction to dynamics of colloids. ISSN. Elsevier Science
31. van Kampen NG. 1986. *J. Stat. Phys.* 44(1-2):1–24
32. Castro-Villarreal P. 2010. *J. Stat. Mech.* 2010(08):P08006
33. Seifert U. 1997. *Adv. Phys.* 46(1):13–137
34. Guven J, Vázquez-Montejo P. 2018. The geometry of fluid membranes: Variational principles, symmetries and conservation laws. Cham: Springer International Publishing, 167–219
35. Gompper G, Dhont J, Elgeti J, Fahlke C, Fedosov D, et al. 2018. 49th iff spring school 2018, physics of life. Jülich Forschungszentrum
36. Heinen M, Schnyder SK, Brady JF, Löwen H. 2015. *Phys. Rev. Lett.* 115(9):097801
37. Southall NT, Dill KA, Haymet ADJ. 2002. *J. Phys. Chem. B* 106(3):521–533
38. Bowick MJ, Giomi L. 2009. *Adv. Phys.* 58(5):449–563
39. Manca F, Déjardin PM, Giordano S. 2016. *Ann. Phys.* 528(5):381–393
40. Polettini M. 2013. *J. Stat. Mech.* 2013(07):P07005
41. Castro-Villarreal P. 2014. *J. Stat. Mech.* 2014(5):P05017
42. Castro-Villarreal P, Solano-Cabrera CO, Castañeda-Priego R. 2023. *Front. Phys.* 11
43. Belloni L. 2000. *J. Condens. Matter Phys.* 12(46):R549–R587
44. Likos CN. 2001. *Phys. Rep.* 348(4):267–439
45. Castañeda Priego R, Rodríguez-López A, Méndez-Alcaraz JM. 2006. *Phys. Rev. E* 73(5):051404
46. Henderson S, Mitchell S, Bartlett P. 2002. *Phys. Rev. Lett.* 88(8):088302
47. Diamant H. 2009. *J. Phys. Soc. Jpn.* 78(4):041002–041002
48. Carbajal-Tinoco MD, Lopez-Fernandez R, Arauz-Lara JL. 2007. *Phys. Rev. Lett.* 99(13):138303

49. Kotar J, Leoni M, Bassetti B, Lagomarsino MC, Cicuta P. 2010. *Proc. Natl. Acad. Sci. USA* 107(17):7669–7673
50. Golestanian R, Yeomans JM, Uchida N. 2011. *Soft Matter* 7:3074
51. Damet L, Cicuta GM, Kotar J, Lagomarsino MC, Cicuta P. 2012. *Soft Matter* 8(33):8672–8678
52. Frenkel D. 2015. *Nat. Mater.* 14:9–12
53. Kondepudi D, Prigogine I. 1998. Modern thermodynamics, from heat engines to dissipative structures. John Wiley and Sons
54. Wang J, Mbah CF, Przybilla T, Englisch S, Spiecker E, et al. 2019. *ACS Nano* 13(8):9005–9015PMID: 31274291
55. Viveros-Méndez PX, Méndez-Alcaraz JM, González-Mozuelos P. 2008. *J. Chem. Phys.* 128(1):014701
56. Viveros-Méndez PX, Méndez-Alcaraz JM, González-Mozuelos P. 2012. *J. Chem. Phys.* 136(16):164902
57. Ramírez-Garza OA, Méndez-Alcaraz JM, González-Mozuelos P. 2021. *Phys. Chem. Chem. Phys.* 23(14):8661–8672
58. Skinner TOE, Aarts DGAL, Dullens RPA. 2010. *Phys. Rev. Lett.* 105(16):168301
59. Bausch AR, Bowick MJ, Cacciuto A, Dinsmore AD, Hsu MF, et al. 2003. *Science* 299(5613):1716–1718
60. Irvine W, Vitelli V, Chaikin P. 2010. *Nature* 468:947 –951
61. Pieranski P, Strzelecki L, Pansu B. 1983. *Phys. Rev. Lett.* 50(12):900–903
62. Vogel N, Utech S, England GT, Shirman T, Phillips KR, et al. 2015. *Proc. Natl. Acad. Sci. USA* 112(35):10845–10850
63. Feng L, Laderman B, Sacanna S, Chaikin P. 2015. *Nat. Mater.* 14:61 –65
64. Chen G, Gallegos MJ, Soetrisno DD, Vekilov PG, Conrad JC. 2024. *Soft Matter* 20:2575 –2583
65. Meng G, Arkus N, Brenner MP, Manoharan VN. 2010. *Science* 327(5965):560–563
66. Griffiths SE, Koumakis N, Brown AT, Vissers T, Warren PB, Poon WCK. 2021. *J. Chem. Phys.* 155(7):074903
67. Sanz E, White KA, Clegg PS, Cates ME. 2009. *Phys. Rev. Lett.* 103(25):255502
68. Spannuth M, Conrad JC. 2012. *Phys. Rev. Lett.* 109(2):028301
69. Li B, Lou K, Kob W, Granick S. 2020. *Nature* 587:225–229
70. Singh N, Sood AK, Ganapthy R. 2020. *Nat. Commun.* 11:4967
71. Ching H, Mohraz A. 2022. *Soft Matter* 18(22):4227–4238
72. Cao C, Huang X, Roth CB, Weeks ER. 2017. *J. Chem. Phys.* 147(22):224505
73. Zhang B, Cheng X. 2016. *Phys. Rev. Lett.* 116(9):098302
74. Marcus AH, Rice SA. 1996. *Phys. Rev. Lett.* 77(12):2577–2580
75. Mermin ND, Wagner H. 1966. *Phys. Rev. Lett.* 17(22):1133–1136
76. Schmidt M, Löwen H. 1996. *Phys. Rev. Lett.* 76(24):4552–4555
77. Neser S, Bechinger C, Leiderer P, Palberg T. 1997. *Phys. Rev. Lett.* 79(12):2348–2351
78. Pansu, B., Pieranski, Pi., Pieranski, Pa. 1984. *J. Phys. France* 45(2):331–339
79. Schmidt M, Löwen H. 1997. *Phys. Rev. E* 55(6):7228–7241
80. Fortini A, Dijkstra M. 2006. *J. Phys.: Condens. Matter* 18(28):L371
81. Manoharan VN. 2006. *Solid State Commun.* 139(11):557–561Soft Condensed Matter
82. Sarangapani PS, Yu Y, Zhao J, Zhu Y. 2008. *Phys. Rev. E* 77(6):061406
83. Cui B, Lin B, Frydel D, Rice SA. 2005. *Phys. Rev. E* 72(2):021402
84. Pandey R, Conrad JC. 2013. *Soft Matter* 9(44):10617–10626
85. Nugent CR, Edmond KV, Patel HN, Weeks ER. 2007. *Phys. Rev. Lett.* 99(2):025702
86. Sarangapani PS, Zhu Y. 2008. *Phys. Rev. E* 77(1):010501
87. Mittal J, Truskett TM, Errington JR, Hummer G. 2008. *Phys. Rev. Lett.* 100(14):145901
88. Watanabe K, Kawasaki T, Tanaka H. 2011. *Nat. Mater.* 10:512–520
89. Hima Nagamanasa K, Gokhale S, Sood A, Ganapathy R. 2015. *Nat. Phys.* 11:403–408

90. Kurzidim J, Coslovich D, Kahl G. 2009. *Phys. Rev. Lett.* 103(13):138303
91. Skinner TOE, Schnyder SK, Aarts DGAL, Horbach J, Dullens RPA. 2013. *Phys. Rev. Lett.* 111(12):128301
92. Ryan C. Roberts Nico Marioni JCP, Conrad JC. 2020. *Mol. Phys.* 118(9-10):e1728407
93. Mandal S, Lang S, Gross M, Oettel M, Raabe D, et al. 2014. *Nat. Commun.* 5(1):1–8
94. Lutz C, Kollmann M, Bechinger C. 2004. *Phys. Rev. Lett.* 93(2):026001
95. Lin B, Meron M, Cui B, Rice SA, Diamant H. 2005. *Phys. Rev. Lett.* 94(21):216001
96. Taloni A, Flomenbom O, Castañeda-Priego R, Marchesoni F. 2017. *Soft Matter* 13(6):1096–1106
97. Cui B, Diamant H, Lin B. 2002. *Phys. Rev. Lett.* 89(18):188302
98. Xu X, Rice SA, Lin B, Diamant H. 2005. *Phys. Rev. Lett.* 95(15):158301
99. Valley DT, Rice SA, Cui B, Ho HM, Diamant H, Lin B. 2007. *J. Chem. Phys.* 126(13):134908
100. Brenner H. 1961. *Chem. Eng. Sci.* 16(3):242–251
101. Lin B, Yu J, Rice SA. 2000. *Phys. Rev. E* 62(3):3909–3919
102. Kluijtmans SGJM, Dhont JKG, Philipse AP. 1997. *Langmuir* 13(19):4982–4987
103. Jacob JDC, He K, Retterer ST, Krishnamoorti R, Conrad JC. 2015. *Soft Matter* 11(38):7515–7524
104. Cui B, Diamant H, Lin B, Rice SA. 2004. *Phys. Rev. Lett.* 92(25):258301
105. Sarangapani PS, Schofield AB, Zhu Y. 2012. *Soft Matter* 8(3):814–818
106. Illing B, Fritschi S, Kaiser H, Klix CL, Maret G, Keim P. 2017. *Proc. Natl. Acad. Sci. USA* 114(8):1856–1861
107. Vivek S, Kelleher CP, Chaikin PM, Weeks ER. 2017. *Proc. Natl. Acad. Sci. USA* 114(8):1850–1855
108. Zhang B, Cheng X. 2019. *Soft Matter* 15(20):4087–4097
109. Roberts RC, Palmer JC, Conrad JC. 2023. *J. Phys. Chem. B* 127(4):961–969PMID: 36656297
110. Huang R, Chavez I, Taute KM, Lukić B, Jeney S, et al. 2011. *Nat. Phys.* 7(7):576–580
111. Li T, Kheifets S, Medellin D, Raizen MG. 2010. *Science* 328(5986):1673–1675
112. Pusey PN. 2011. *Science* 332(6031):802–803
113. Harano K. 2021. *Bull. Chem. Soc. Jpn.* 94(2):463–472
114. Blair DL, Kudrolli A. 2003. *Phys. Rev. E* 67(2):021302
115. Abate AR, Durian DJ. 2008. *Phys. Rev. Lett.* 101(24):245701
116. Abate AR, Durian DJ. 2006. *Phys. Rev. E* 74(3):031308
117. González-Gutiérrez J, Carrillo-Estrada JL, Ruiz-Suárez JC. 2013. *J. Phys. Conf. Ser.* 475(1):012003
118. Sperl M, Zippelius A. 2017. *Eur. Phys. J.: Spec. Top.* 226(14):3079–3094
119. Russo KI, Merlino A, Vergara A, Sica F. 2013. *Int. J. Mol. Sci.* 14(6):11643–91
120. Smeets B, Pešek J, Deckers T, Hall GN, Cuvelier M, et al. 2020. *Matter* 2(5):1283–1295
121. Rahbari SHE, Vollmer J, Herminghaus S, Brinkmann M. 2010. *Phys. Rev. E* 82(6):061305
122. Sapozhnikov MV, Tolmachev YV, Aranson IS, Kwok WK. 2003. *Phys. Rev. Lett.* 90(11):114301
123. Grzybowski BA, Wiles JA, Whitesides GM. 2003. *Phys. Rev. Lett.* 90(8):083903
124. Grzybowski BA, Wilmer CE, Kim J, Browne KP, Bishop KJM. 2009. *Soft Matter* 5(6):1110–1128
125. Rietz F, Radin C, Swinney HL, Schröter M. 2018. *Phys. Rev. Lett.* 120(5):055701
126. Escobar A, Tapia-Ignacio C, Donado F, Arauz-Lara JL, Moctezuma RE. 2020. *Phys. Rev. E* 101(5):052907
127. Grzybowski BA, Stone HA, Whitesides GM. 2000. *Nature* 405(6790):1033–1036
128. Helgesen G, SvÃ¥sand E, Skjeltorp AT. 2008. *J. Condens. Matter Phys.* 20(20):204127
129. Daniels KE, Behringer RP. 2005. *Phys. Rev. Lett.* 94(16):168001
130. Maaß CC, Isert N, Maret G, Aegerter CM. 2008. *Phys. Rev. Lett.* 100(24):248001
131. Lim MX, Souslov A, Vitelli V, Jaeger HM. 2019. *Nat. Phys.* 15(5):460–464

132. Donado F, Moctezuma RE, López-Flores L, Medina-Noyola M, Arauz-Lara JL. 2017. *Sci. Rep.* 7(1):12614
133. Tapia-Ignacio C, Garcia-Serrano J, Donado F. 2016. *Phys. Rev. E* 94(6):062902
134. Tapia-Ignacio C, Moctezuma RE, Donado F. 2018. *Phys. Rev. E* 98(3):032901
135. Escobar A, Ledesma-Motolinía M, Carrillo-Estrada JL, Donado F. 2023. *Sci. Rep.* 13(1):8552
136. Russo J, Tanaka H. 2016. *J. Chem. Phys.* 145(21):211801
137. Zhang TH, Liu XY. 2007. *Journal of the American Chemical Society* 129(44):13520–13526PMID: 17929918
138. Savage JR, Dinsmore AD. 2009. *Phys. Rev. Lett.* 102(19):198302
139. Fang H, Hagan MF, Rogers WB. 2020. *Proc. Natl. Acad. Sci. USA* 117(45):27927–27933
140. Escobar A, Donado F, Moctezuma RE, Weeks ER. 2021. *Phys. Rev. E* 104(4):044904
141. Ledesma-Motolinía M, Carrillo-Estrada JL, Escobar A, Donado F, Castro-Villarreal P. 2023. *Phys. Rev. E* 107(2):024902
142. Carmo MD. 1976. Differential geometry of curves and surfaces. Prentice-Hall, 1st ed.
143. Ledesma-Durán A, Juárez-Valencia LH. 2023. *Eur. Phys. J. E* 46(8):70
144. Castro-Villarreal P, Villada-Balbuena A, Méndez-Alcaraz JM, Castañeda-Priego R, Estrada-Jiménez S. 2014. *J. Chem. Phys.* 140(21):214115
145. Gardiner C. 2009. Stochastic methods: A handbook for the natural and social sciences. Springer Series in Synergetics. Springer Berlin Heidelberg
146. Villada-Balbuena A, , Ortiz-Ambriz A, Castro-Villarreal P, Tierno P, et al. 2021. *Phys. Rev. Res.* 3(3):033246
147. Castro-Villarreal P, Sevilla FJ. 2018. *Phys. Rev. E* 97(5):052605
148. Apaza L, Sandoval M. 2018. *Soft Matter* 14(48):9928–9936
149. Ramírez-Garza OA, Méndez-Alcaraz JM, González-Mozuelos P. 2017. *J. Chem. Phys.* 146(19):194903
150. Solano-Cabrera CO, Castañeda-Priego R, Castro-Villarreal P. 2024. *To be submitted.*
151. Cavallaro M, Botto L, Lewandowski EP, Wang M, Stebe KJ. 2011. *Proc. Natl. Acad. Sci. USA* 108(52):20923–20928
152. van Blaaderen A. 2003. *Science* 301(5632):470–471
153. Manoharan VN, Elsesser MT, Pine DJ. 2003. *Science* 301(5632):483–487
154. Li W, Palis H, Mérindol R, Majimel J, Ravaine S, Duguet E. 2020. *Chem. Soc. Rev.* 49(6):1955–1976